SECURITY

AD-A239 248

IT DOCUMENTATION PAGE

1a. REP

1b. RESTRICTIVE MARKINGS

2a. SECURITY CLASSIFICATION AUTHORITY

3. DISTRIBUTION / AVAILABILITY OF REPORT
APPROVED FOR PUBLIC RELEASE:
DISTRIBUTION UNLIMITED

2b. DECLASSIFICATION / DOWNGRADING SCHEDULE

4. PERFORMING ORGANIZATION REPORT NUMBER(S)
ONR TECHNICAL REPORT #

5. MONITORING ORGANIZATION REPORT NUMBER(S)

6a. NAME OF PERFORMING ORGANIZATION
UNIVERSITY OF UTAH

6b. OFFICE SYMBOL (If applicable)

7a. NAME OF MONITORING ORGANIZATION
OFFICE OF NAVAL RESEARCH
CHEMISTRY PROGRAM

6c. ADDRESS (City, State, and ZIP Code)
DEPARTMENT OF CHEMISTRY
UNIVERSITY OF UTAH
SALT LAKE CITY, UTAH 84112

7b. ADDRESS (City, State, and ZIP Code)

8a. NAME OF FUNDING / SPONSORING ORGANIZATION
OFFICE OF NAVAL RESEARCH

8b. OFFICE SYMBOL (If applicable)
ONR

9. PROCUREMENT INSTRUMENT IDENTIFICATION NUMBER
N00014-89-J-1497

8c. ADDRESS (City, State, and ZIP Code)
800 NORTH QUINCY STREET
ARLINGTON, VA 22217-5000

10. SOURCE OF FUNDING NUMBERS

PROGRAM ELEMENT NO.	PROJECT NO.	TASK NO.	WORK UNIT ACCESSION NO

11. TITLE (Include Security Classification)
An Initio Studies of Ground and Excited Electronic States of MgAr, CdAr, and BeAr
(unclassified)

12. PERSONAL AUTHOR(S)
Jerry A. Boatz, Keld Lars Bak, and Jack Simons

13a. TYPE OF REPORT	13b. TIME COVERED	14. DATE OF REPORT (Year, Month, Day)	15. PAGE COUNT
TECHNICAL	FROM _____ TO _____	July 26, 1991	34

16. SUPPLEMENTARY NOTATION

17 COSATI CODES			18. SUBJECT TERMS (Continue on reverse if necessary and identify by block number)
FIELD	GROUP	SUB-GROUP	

19. ABSTRACT (Continue on reverse if necessary and identify by block number)

(See reverse.)

20. DISTRIBUTION / AVAILABILITY OF ABSTRACT
☐ UNCLASSIFIED/UNLIMITED ☐ SAME AS RPT ☐ DTIC USERS

21. ABSTRACT SECURITY CLASSIFICATION
UNCLASSIFIED

22a. NAME OF RESPONSIBLE INDIVIDUAL	22b. TELEPHONE (Include Area Code)	22c. OFFICE SYMBOL
JACK SIMONS	(801) 581-8023	

DD FORM 1473, 84 MAR

83 APR edition may be used until exhausted

ABSTRACT

The ground state ($X\ ^1\Sigma^+$) and several excited state ($A\ ^3\Pi$, $c\ ^3\Sigma^+$, $C\ ^1\Pi$, $D\ ^1\Sigma^+$, and $E\ ^3\Sigma^+$) potential energy surfaces for the diatomic molecules MgAr, CdAr, and BeAr have been computed using complete active space self-consistent field (CASSCF) wavefunctions and valence double- and triple-zeta quality basis sets augmented with polarization and diffuse functions. Pump-and-probe laser experiments have examined the quenching of excited singlet states of metal-rare gas complexes such as CdXe to produce triplets that dissociate to ^3P_J metal atoms. This quenching, which is detected for CdXe but not for CdAr or MgAr, is thought to occur via a crossing or strong coupling of a repulsive triplet curve with an attractive singlet curve. The present work indicates that the attractive $C\ ^1\Pi$ and repulsive $c\ ^3\Sigma^+$ curves of MgAr and CdAr do not intersect in the energetically accessible region of the $C\ ^1\Pi$ surface, unlike the corresponding curves for the CdXe diatom. These data are consistent with the absence of ^3P_J Mg and ^3P_J Cd atoms in the MgAr and CdAr experiments, respectively. However, an alternative quenching mechanism involving "vibronic" coupling between the $C\ ^1\Pi$ vibrational eigenstates and the continuum eigenstates of the underlying repulsive $^3\Sigma^+$ surface may be operative; this possibility is examined and predicted to be unlikely for MgAr (due to small spin-orbit coupling) and CdAr (due to unfavorable vibronic factors). BeAr, which has yet to be probed experimentally, is predicted to be bound by 770 and 900 cm^{-1} in the $D\ ^1\Sigma^+$ and $E\ ^3\Sigma^+$ states, respectively, and to display interesting potential curve intersections.

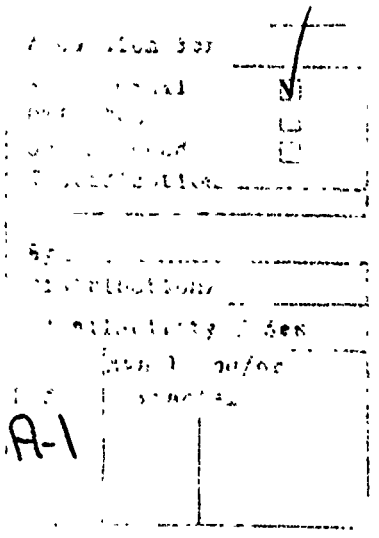

OFFICE OF NAVAL RESEARCH

Contract N00014-89-J-1497

R&T Code 413050. . .02

Technical Report No. 20

An Initio Studies of Ground and Excited Electronic States of MgAr, CdAr, ai.d BeAr

by
Jerry A. Boatz, Keld Lars Bak, and Jack Simons

Prepared for Publication in

Theoretica Chimica Acta

The University of Utah
Department of Chemistry
Salt Lake City, Utah 84112-1194

July 1991

Ab Initio Studies of Ground and Excited Electronic States of MgAr, CdAr, and BeAr

Jerry A. Boatz,[a] Keld Laia Bak,[b] and Jack Simons*

Department of Chemistry

University of Utah

Salt Lake City, UT 84112

[a] Present Address:

Phillips Laboratory

Astronautical Sciences Division

Edwards Air Force Base, CA 93523

[b] Present Address:

Department of Chemistry

Aarhus University

DK-8000 Aarhus C, Denmark

ABSTRACT

The ground state ($X\ ^1\Sigma^+$) and several excited state ($A\ ^1\Pi$, $c\ ^3\Sigma^+$, $C\ ^1\Pi$, $D\ ^1\Sigma^+$, and $E\ ^3\Sigma^+$) potential energy surfaces for the diatomic molecules MgAr, CdAr, and BeAr have been computed using complete active space self-consistent field (CASSCF) wavefunctions and valence double- and triple-zeta quality basis sets augmented with polarization and diffuse functions. Pump-and-probe laser experiments have examined the quenching of excited singlet states of metal-rare gas complexes such as CdXe to produce triplets that dissociate to ^3P_J metal atoms. This quenching, which is detected for CdXe but not for CdAr or MgAr, is thought to occur via a crossing or strong coupling of a repulsive triplet curve with an attractive singlet curve. The present work indicates that the attractive $C\ ^1\Pi$ and repulsive $c\ ^3\Sigma^+$ curves of MgAr and CdAr do not intersect in the energetically accessible region of the $C\ ^1\Pi$ surface, unlike the corresponding curves for the CdXe diatom. These data are consistent with the absence of ^3P_J Mg and ^3P_J Cd atoms in the MgAr and CdAr experiments, respectively. However, an alternative quenching mechanism involving "vibronic" coupling between the $C\ ^1\Pi$ vibrational eigenstates and the continuum eigenstates of the underlying repulsive $^3\Sigma^+$ surface may be operative; this possibility is examined and predicted to be unlikely for MgAr (due to small spin-orbit coupling) and CdAr (due to unfavorable vibronic factors). BeAr, which has yet to be probed experimentally, is predicted to be bound by 770 and 900 cm^{-1} in the $D\ ^1\Sigma^+$ and $E\ ^3\Sigma^+$ states, respectively, and to display interesting potential curve intersections.

I. Introduction

The alkaline earth-rare gas and other similar van der Waals diatomic systems have been the focus of several recent experimental[1-7] and theoretical[8-14] studies. Of primary interest in these works is the characterization of both the weakly-bound van der Waals ground-state complex[3,6-10,14] and low-lying singlet and triplet excited state[1-7,10-13] potential energy surfaces of these molecules.

Experimental studies of MgAr[3] and CdAr[6] (as well as other similar systems[2c,2d]) indicate that the binding on the ground state potential energy surface is primarily due to a weak van der Waals interaction and produces large equilibrium internuclear distances (r_e = 4.49 and 4.33 Å, respectively.) In contrast, the C $^1\Pi$ and A $^3\Pi$ states of MgAr are bound by over 300 cm^{-1} and have considerably smaller r_e's (3.27 and 3.63 Å, respectively.)[4] Furthermore, the E $^3\Sigma^+$ Rydberg state (e.g., having appreciable $(3s)^1(4s)^1$ character for MgAr) is bound by over 1100 cm^{-1} (see Figure 1a.) The presence of minima on these potential energy surfaces can be understood in terms of an ion-induced dipole model in which the rare gas atom is attracted to a partially shielded Mg^+ ion core. In the Π states, the Π orientation of the singly-occupied p orbital on Mg allows for a closer approach of the rare gas atom than when the p orbital is in the Σ orientation.[3] Similarly, in the Rydberg state, provided the approaching rare-gas atom penetrates the spatially diffuse Rydberg orbital (which induces a slight initial repulsion at long internuclear distances), it will be again be attracted to a partially shielded Mg^+ ion core.

In the laser pump-probe experiments,[2,3,6,7] X $^1\Sigma^+$ ground-state metal-rare gas (i.e., M•RG) molecules are excited to the $^1\Pi$ surface and subsequent appearance of ^3P_J M atoms is monitored. Production of triplet M is thought to occur via crossing of the repulsive c $^3\Sigma^+$ state and the initially populated C $^1\Pi$ state.

That is, the lower-lying repulsive c $^3\Sigma^+$ state (which correlates at infinite separation with ^3P M + ^1S Ar) intersects an energetically accessible region of the bound C $^1\Pi$ state. This supposition is primarily based upon experimental studies of the CdXe diatom, where production of the C $^1\Pi$ state leads to efficient production of ^3P_J Cd atoms via a spin-orbit coupling between the bound C $^1\Pi$ state and the dissociative c $^3\Sigma^+$ state.[7] Indeed, virtually no fluorescence from the C $^1\Pi$ state is observed at all in CdXe. However, in analogous experiments on CdAr,[6] just the opposite occurs; namely, fluorescence of the C $^1\Pi$ state is prevalent, with no detectable formation of ^3P_J Cd atoms. This is rather puzzling, since it seems reasonable to expect the potential curves and the strength of the spin-orbit coupling of CdXe and CdAr to be quite similar. Likewise, no production of ^3P_J Mg atoms is observed after the formation of C $^1\Pi$ MgAr,[3] although this is less surprising since the spin-orbit coupling in Mg is considerably less than that in Cd.

Prior theoretical studies of MgAr include the all-electron fourth-order Møller-Plesset calculations[9] on the ground state and the perturbative calculations[10] of the dispersion energies of the lowest singlet and triplet Σ, Π, and Δ excited states (as well as the ground state.) Similar calculations have been performed for CdAr[12] and related systems.[12,13] Apparently, the only prior calculation on BeAr has been a rather approximate calculation of its ground state potential energy surface, at the SCF level.[14]

The purpose of the present work is to investigate the validity of the physical pictures introduced above and to identify regions of surface intersections and/or avoided crossings for the molecules MgAr, CdAr, and BeAr. To this end, *qualitatively* correct potential energy surfaces are calculated for the electronic states of interest.

II. Computational Methods

In order to obtain a balanced description of all electronic states considered here, complete active space self-consistent field (CASSCF) wavefunctions were employed. The active space consisted of the two 3s electrons of Mg, distributed in all possible ways among the 3s, 3p, 4s, and 4p Mg orbitals. This space generates 16, 8, 8, and 8 configuration state functions (CSFs) of $^1\Sigma^+$, $^3\Sigma^+$, $^1\Pi$, and $^3\Pi$ symmetry, respectively. It should be noted that not including any of the electrons and orbitals on Ar in the active space excludes from the calculation those CSFs required to describe dispersion interactions, which are necessary for quantitatively accurate calculations of weak intermolecular interactions (such as van der Waals). Hence, these calculations cannot predict the presence of shallow wells in the X $^1\Sigma^+$, C $^1\Pi$, A $^3\Pi$, and E $^3\Sigma^+$ states. However, the primary objective of this study is not a quantitatively accurate description of well depths and bond lengths; these data are much more accurately known from interpretations of the experimental data. Rather, we are seeking a qualitatively correct picture of the individual potential energy surfaces which will allow us to identify, among other features, probable regions of intersections and/or avoided crossings between electronic states.

The basis sets used in this study are summarized in Table I. For all three molecules, the effective core potential (ECP) and the companion valence double-zeta basis set of Stevens, Basch, and Krauss[15] were used for Ar. The valence basis was augmented with a single set of diffuse s and p functions as well as two sets of five d-type polarization functions. (See Table I for the values of the exponents used.) In order to test the validity of using an effective core potential on Ar, the calculations of all the potential energy curves of BeAr were repeated using an all-electron treatment of Ar. Virtually identical

potential energy curves are obtained for all of the electronic states. For the all-electron calculations, the Ar basis consisted of the McLean-Chandler (12s9p/6s5p) set[16] plus the same set of diffuse and polarization functions used in the ECP computations.

For each of the metal atoms considered in this work, the basis set used is constructed in a similar manner. Starting with a basis set which is at least of valence double-zeta quality, a single set of five d-type polarization functions are added. Next, in order to have a basis set which is sufficiently flexible to describe the triplet (ns)([n+1]s) Rydberg states (i.e., E $^3\Sigma^+$), two sets of diffuse s and p functions are added (see Table I for the exponents.) An exception is made for cadmium, for which only a single set of diffuse s and p functions were added. For magnesium, the McLean-Chandler (12s9p/6s5p) basis set[16] is used. The 6-311G basis set of Pople et al.[17] is used for beryllium. The ECP of Hay and Wadt[18] and the associated double-zeta valence basis set is used for cadmium. The MESSKIT[19] suite of computer programs was used in performing all energy calculations. All calculated potential energy curves were corrected for basis set superposition error using the counterpoise method of Boys and Bernardi.[20]

III. Results and Discussion

In order to compare the present calculations with experiment, the atomic energies of the metal atoms for the states which correlate to the X $^1\Sigma^+$, A $^3\Pi$, c $^3\Sigma^+$, C $^1\Pi$, D $^1\Sigma^+$, and E $^3\Sigma^+$ states of the M•RG complexes were calculated, using the same active space and basis sets as outlined in the previous section. The results are summarized in Table II. With the exception of the Be ^1S -> ^1P transition energy (which is about 0.9 eV too high), all calculated transition energies agree to within approximately 0.5 eV of the experimental values.

For ease of chemical interpretation, Table III summarizes the relationship between the spectroscopic notation for each electronic state and the dominant electron configuration, in terms of the orbitals on the metal atom.

The calculated potential energy curves for MgAr, CdAr, and BeAr are shown in Figures 1a, 1b, and 1c, respectively. (No local minima are observed in any of the MgAr and CdAr curves, in contrast to experimental findings. As mentioned earlier, this is to be expected based upon the nature of the present calculations and is of minor significance in regard to the objectives of this paper.)

MgAr: Figure 1a shows that the X $^1\Sigma^+$ potential remains "flat" until the internuclear distance R decreases to about 4 Å, after which it rises quite sharply. The A $^3\Pi$ and c $^3\Sigma^+$ states, which are degenerate at R = ∞, remain nearly so until R decreases to about 5 Å. At this point, the c $^3\Sigma^+$ surface begins to rise in energy while the A $^3\Pi$ state remains level until R shrinks to near 4 Å. Similar behavior is observed for the C $^1\Pi$ and D $^1\Sigma^+$ states (which are also degenerate at infinite separation, in the absence of spin-orbit coupling), although the C $^1\Pi$ state is less strongly repulsive than its triplet counterpart. These observations are consistent with the fractional charge-induced dipole model,[3] which states that the Π orientation of the singly-occupied p orbital on Mg allows for a closer approach of the argon atom than does the Σ orientation. Finally, the E $^3\Sigma^+$ Rydberg state remains level until R decreases to near 3 Å, and thus behaves similarly to the Π states.

Of particular interest in Figure 1a are the relative locations of the C $^1\Pi$ and c $^3\Sigma^+$ curves. Based on experimental studies of CdXe,[7] it might be anticipated that these two curves intersect in an energetically accessible region of the C $^1\Pi$ surface; i.e., at an energy below the asymptotic limit of ^{1}P

Mg + ^{1}S Ar. Inspection of Figure 1a shows that these curves intersect well above this limit. In Figure 2a, the C $^1\Pi$ and c $^3\Sigma^+$ curves have been shifted so that the asymptotic ^{1}P Mg + ^{1}S Ar and ^{3}P Mg + ^{1}S Ar energies match the experimental values. Even so, the intersection of these two curves still occurs far above the asymptotic ^{1}P Mg + ^{1}S Ar limit. While it is possible that the level of calculation here is inadequate to correctly describe the behavior of the C $^1\Pi$ and c $^3\Sigma^+$ states for small internuclear distances, it is also possible that a mechanism other than curve crossing exists whereby a spin-orbit assisted transition between these two states can take place. Although it seems unlikely that these curves actually intersect at an energy below that of ^{1}P Mg + ^{1}S Ar, it seems quite probable that these curves will closely approach each other for energies near this energy limit. This, in turn, could allow for a large overlap between the vibrational eigenstates of the bound C $^1\Pi$ state with the isoenergetic continuum eigenstates of the repulsive c $^3\Sigma^+$ state. This possibility will later be explored in greater detail (*vide infra*).

CdAr: The computed potential energy curves of CdAr are found in Figure 1b and are quite similar to those of MgAr (see Figure 1a). As in MgAr, the ground state potential starts to rise in the vicinity of R = 4 Å. However, both the c $^3\Sigma^+$ and D $^1\Sigma^+$ curves become repulsive at a slightly larger internuclear distance (near R = 5 Å) relative to MgAr.

Inspection of Figure 1b shows that the c $^3\Sigma^+$ and C $^1\Pi$ curves intersect at an energy well above the ^{1}P Cd + ^{1}S Ar limit. This is still true even after these curves have been shifted so that the asymptotic energies match those of experiment (see Figure 2b.) Since the c $^3\Sigma^+$ and C $^1\Pi$ states seem likely not to intersect at an energy below ^{1}P Cd + ^{1}S Ar, the same vibronic interaction mechanism outlined above may again be the primary means of a spin-orbit assisted transition between these two curves (*vide infra*).

BeAr: Figure 1c shows the calculated potential energy curves of BeAr. These surfaces exhibit the same general characteristics of those for MgAr and Cdar; namely, that the c $^3\Sigma^+$ and D $^1\Sigma^+$ curves become repulsive at longer R than do their Π counterparts and that an intersection of the c $^3\Sigma^+$ and C $^1\Pi$ curves at an energy below ^{1}P Be + ^{1}S Ar seems improbable. Unlike MgAr and CdAr, however, the calculated potential energy curves for BeAr show the presence of local minima in the D $^1\Sigma^+$ and E $^3\Sigma^+$ curves, with well depths of approximately 770 and 900 cm^{-1}, respectively. The former apparently is caused by an avoided crossing with a higher state of $^1\Sigma^+$ symmetry (not shown in Figure 1c.) The presence of a well on the E $^3\Sigma^+$ Rydberg surface is consistent with the fractional charge - induced dipole model as discussed in the Introduction. The "shoulder" on the repulsive limb of the c $^3\Sigma^+$ curve is apparently the result of an avoided crossing with the higher-lying E $^3\Sigma^+$ state. Note that in the region of this avoided crossing, the c $^3\Sigma^+$ state is diverted away from the C $^1\Pi$ curve. Consequently, if the latter two curves intersect, the point of intersection will occur at a smaller internuclear distance (and hence at a higher energy) than if the avoided crossing was absent.

As seen in Figure 1c, the calculated c $^3\Sigma^+$ and C $^1\Pi$ curves of BeAr do not intersect below the ^{1}P Be + ^{1}S Ar energy. However, when these two curves are shifted to match the corresponding experimental asymptotic energies, their intersection occurs at an energy near the asymptotic limit (see Figure 2c.) This is in contrast to the analogous curves of MgAr and CdAr and suggests that, in the case of BeAr, predissociation to the c $^3\Sigma^+$ state from the C $^1\Pi$ surface may indeed take place via an actual curve crossing, rather than by a vibronic mechanism (*vide infra.*)

In Figure 2c, all of the calculated potential energy curves of BeAr have been shifted so that their asymptotic energies match the corresponding

experimental atomic energies of the Be atom. We believe that this gives a reasonably accurate picture of the ground and low-lying excited states of BeAr, and so the potential energy surfaces in Figure 2c will form the basis of our discussion on the experimental implications of the wells on the D $^1\Sigma^+$ and E $^3\Sigma^+$ surfaces.

The presence of these wells is intriguing and suggests that these excited states of BeAr may be detectable in laser pump-probe experiments similar to those performed on MgAr[3,4] and CdAr.[5,6] In particular, if a metastable triplet BeAr complex on the (presumably bound) A $^3\Pi$ surface can be prepared in a supersonic jet expansion (as is done for MgAr[4]), then laser excitation to the bound E $^3\Sigma^+$ Rydber- state should be possible. Furthermore, once triplet Rydberg BeAr has been prepared, several routes may then be taken to other states. Since the c $^3\Sigma^+$ and E $^3\Sigma^+$ states undergo an avoided crossing in the vicinity of the E $^3\Sigma^+$ minimum, a radiationless transition back to the c $^3\Sigma^+$ surface is possible. Note, however, that the degree to which these two states avoid each other is probably overemphasized in Figure 2c. This is because the energy spacing of the corresponding unshifted curves in Figure 1c (from which the curves in Figure 2c are obtained) is somewhat smaller than indicated by the experimental Be atomic excitation energies.

Because the spin-orbit coupling is small for beryllium, a spin-forbidden transition from the E $^3\Sigma^+$ Rydberg state of BeAr to the underlying D $^1\Sigma^+$ state is unlikely to occur to a significant extent. However, such a transition could allow for the characterization of both the short-range attractive and long-range repulsive regions of the D $^1\Sigma^+$ surface.

Vibronic Coupling: Although the c $^3\Sigma^+$ and C $^1\Pi$ curves of MgAr and CdAr apparently do not intersect at an energy below the ^{1}P Mg + ^{1}S Ar and ^{1}P Cd + ^{1}S

Ar asymptotic limits, respectively, there still may exist other means by which these two potential energy surfaces can interact. Since these two curves are in close proximity at small internuclear distances, a possible mechanism is for a "vibronic" coupling between the bound vibrational eigenstates of the C $^1\Pi$ state and the continuum eigenstates of the unbound c $^3\Sigma^+$ state. This kind of coupling is illustrated in Figure 3, which shows a vibrational eigenfunction of a Morse potential[21] and the isoenergetic continuum eigenfunction of the underlying repulsive triplet curve superimposed on their respective potential energy surfaces. The net overlap of these two eigenfunctions serves as an indication of the likelihood of a connecting vibronic interaction. Since the continuum eigenstate oscillates much more rapidly than does the Morse potential eigenstate, the overlap of these two functions is expected to be virtually zero, with the possible exception of the region of the repulsive "wall" where the two potential energy curves are in close proximity. In this region, the rate of oscillation of the continuum eigenfunction is somewhat reduced, which may allow for a nonzero overlap with the innermost "envelope" of the Morse potential eigenfunction.

In order to investigate the likelihood for such vibronic couplings in MgAr and CdAr, the C $^1\Pi$ states of these diatomics were modelled using Morse potentials, with the Morse parameters determined from fits to experimental data.[3,6] Our calculated triplet curves in Figures 2a and 2b were used to represent the underlying c $^3\Sigma^+$ states. Then, for each experimentally observed vibrational level of the bound C $^1\Pi$ state, the corresponding Morse vibrational eigenfunction was computed. At the corresponding energy on the underlying c $^3\Sigma^+$ state, the continuum nuclear wavefunction was then calculated. (Since the continuum eigenfunctions of MgAr and CdAr do not approach zero in the limit of large internuclear distances, they were "box-normalized" using an arbitrary

length L which extended well beyond the outer envelopes of all of the Morse potential eigenfunctions calculated here.) Finally, the overlap was computed via numerical integration of the product of these two nuclear wavefunctions.

In MgAr, there are eight (v=0-7) vibrational levels observed in the C $^1\Pi$ state.[3] Figures 4a and 4b are plots of the v=0 and v=7 vibrational eigenfunctions, respectively, of the C $^1\Pi$ state of MgAr superimposed with the corresponding isoenergetic continuum eigenfunctions of the underlying unbound c $^3\Sigma^+$ state. Of particular importance in these plots is the relative position of the innermost envelopes of the Morse eigenfunction and the continuum eigenfunction, since the total overlap is determined primarily by the degree of overlap of these two envelopes. For the v=0 level of C $^1\Pi$ MgAr (Figure 4a), the innermost envelope of the continuum eigenfunction occurs well before that of the Morse eigenfunction. Therefore, a small overlap is anticipated for this vibrational level. However, for v=7 (Figure 4b), one observes a significant non-zero overlap of the respective innermost envelopes and therefore a relatively large total overlap is expected.

The results of the numerical integrations of the Morse potential eigenfunctions with the corresponding continuum eigenfunctions for all eight vibrational levels of MgAr are summarized in Table IV. There are two sets of values listed in Table IV. One set consists of the actual overlap magnitudes and the other set is the percentages of the maximum possible overlaps. The maximum overlap is defined as the overlap which occurs when the c $^3\Sigma^+$ state intersects the C $^1\Pi$ state *at the energy of the particular C $^1\Pi$ vibrational level*. The data in Table IV shows that both the overlap magnitudes and percentages increase with increasing vibrational quantum number. This implies that the C $^1\Pi$ and c $^3\Sigma^+$ curves are becoming closer as the vibrational energy of

the C $^1\Pi$ state increases and that there is a concomitant increase in the likelihood of a vibronic coupling of these two states.

There are twelve observed vibrational levels (v=0-11) for CdAr.[6] Figures 5a and 5b are plots of the v=0 and v=11 vibrational eigenfunctions, respectively, of the C $^1\Pi$ state superimposed on the corresponding continuum eigenfunctions of the underlying c $^3\Sigma^+$ state. Note that the oscillations of the continuum eigenfunctions are more rapid for CdAr than for MgAr. This is due to the larger ^1P - ^3P energy difference in Cd (1.69 eV) relative to Mg (1.65 eV). Similar to MgAr, the v=0 plot (Figure 5a) shows virtually zero overlap of the innermost envelopes of the respective eigenfunctions. However, even for v=11, there is still very little overlap of the inner envelopes (see Figure 5b). Table V summarizes the computed overlaps and the maximum overlap percentages for each of the twelve observed vibrational levels of C $^1\Pi$ CdAr. As in MgAr, both the overlap magnitudes and percentages increase with increasing vibrational quantum number. However, both sets of data are significantly smaller than their MgAr counterparts. This indicates (ignoring the difference in magnitude of Cd and Mg spin-orbit couplings) that CdAr is less likely to undergo a vibronic coupling of the C $^1\Pi$ and c $^3\Sigma^+$ states than is MgAr.

IV. Conclusions

This paper has attempted to provide a detailed look at the ground state and several of the excited state potential curves of the diatomic molecules MgAr, CdAr, and BeAr. In contrast to implications from experimental studies of CdXe, the computed potentials show no intersection of the C $^1\Pi$ and c $^3\Sigma^+$ states in regions below the energetically accessible ^1P Mg (or ^1P Cd) + ^1S Ar limit. A mechanism involving "vibronic" coupling of the vibrational eigenstates of the C $^1\Pi$ state and the continuum eigenstates of the underlying c $^3\Sigma^+$ state is proposed

as an alternative means of intersystem crossing in MgAr and CdAr. Calculation of the overlap of the nuclear wavefunctions of the c $^3\Sigma^+$ and C $^1\Pi$ states suggest that this type of vibronic coupling is more likely to take place in MgAr than CdAr; of course, spin-orbit coupling is larger in the CdAr case than for MgAr. The overall intersystem crossing rate is expected to depend on the product of spin-orbit factors and a vibronic factor and thus to be small for both MgAr (due to the small spin-orbit factor) and CdAr (due to the small vibronic factor).

The D $^1\Sigma^+$ and E $^3\Sigma^+$ states of BeAr are predicted to be bound by 770 and 900 cm^{-1}, respectively, and thus may constitute interesting synthetic targets for the experimentalist.

Acknowledgements

This work was supported through National Science Foundation Grant CHE 881475 and by The Office of Naval Research. The authors would like to acknowledge several enlightening discussions with Professor W. Breckenridge and Dr. Ingvar Wallace and the technical assistance of Dr. Maciej Gutowski.

References

1. Duval, M.-C.; D'Azy, O.B.; Breckenridge, W.H.; Jouvet, C.; Soep, B. *J. Chem. Phys.* 1986, 85, 6324-6334.

2. a) Breckenridge, W.H.; Merrow, C.N. *J. Chem. Phys.* 1988, 88, 2329-2333.
   b) Kolwaski, A.; Funk, D.J.; Breckenridge, W.H. *Chem. Phys. Lett.* 1986, 132, 263-268.
   c) Breckenridge, W.H.; Merrow, C.N. *J. Chem. Phys.* 1988, 88, 2320-2328.
   d) Wallace, I.; Bennett, R.R.; Breckenridge, W.H. *Chem. Phys. Lett* 1988, 153, 127-132.

3. Bennett, R.R.; McCaffrey, J.G.; Wallace, I.; Funk, D.J.; Kowalski, A.; Breckenridge, W.H. *J. Chem. Phys.* 1989, 90, 2139-2147.

4. Bennett, R.R.; McCaffrey, J.G.; Breckenridge, W.H. *J. Chem. Phys.* 1990, 92, 2740-2747.

5. Kvaran, A.; Funk, D.J.; Kowalski, A.; Breckenridge, W.H. *J. Chem. Phys.* 1988, 89, 6069-6080.

6. Funk, D.J.; Kvaran, A.; Breckenridge, W.H. *J. Chem. Phys* 1989, 90, 2915-2926.

7. Funk, D.J.; Breckenridge, W.H. *J. Chem. Phys.* 1989, 90, 2927-2934.

8. Pouilly, B.; Lengsfield, B.H.; Yarkony, D.R. *J. Chem. Phys.* 1984, 80, 5089-5094.

9. Funk, D.J.; Breckenridge, W.H.; Simons, J.; Chalasiński, G. *J. Chem. Phys.* 1989, 91, 1114-1120.

10. Hliwa, M.; Daudey, J.-P. *Chem. Phys. Lett.* 1988, 153, 471-476.

11. Okunishi, M.; Yamanouchi, K.; Tsughiyo, S. *Chem. Lett.* 1989, 393-396.

12. Czuchaj, E.; Sienkiewicz, J. *J. Phys. B.* 1994, 17, 2251.

13. Czuchaj, E.; Stoll, H.; Preuss, H. *J. Phys. B* 1987, 20, 1487.

14. Kaufmann, J.J. *J. Chem. Phys.* 1973, 58, 4880-4890.

15. Stevens, W.J.; Basch, H.; Krauss, M. *J. Chem. Phys.* 1984, 81, 6026-6033.

16. McLean, A.D.; Chandler, G.S. *J. Chem. Phys.* 1980, 72, 5639-5648.

17. Krishnan, R.; Binkley, J.S.; Seeger, R.; Pople, J.A. *J. Chem. Phys.* 1980, 72, 650-654.

18. Hay, P.J.; Wadt, R.J. *J. Chem. Phys.* 1985, 82, 270-283.

19. The Utah MESS-KIT is a suite of highly modular codes that were programmed in-house to give a variety of electronic structure functionalities by J.A. Nichols, M.R. Hoffmann, R.A. Kendall, H.L. Taylor, D.W. O'Neal, E. Earl, R. Hernandez, M. Gutowski, J. Boatz, K. Bak, J. Anchell, X. Wang, M. Feyereisen, and J. Simons.

20. Boys, S.F.; Bernardi, F. *Mol. Phys.* **1970**, 19, 553.

21. Morse, P.M. *Phys. Rev.* **1929**, 34, 57.

Figure Captions

1a. Calculated potential energy surfaces of MgAr, with the experimentally determined equilibrium bond lengths denoted "Re" and the ground-state v=0 turning points shown by ().

1b. Calculated potential energy surfaces of CdAr, with the experimentally determined equilibrium bond lengths denoted "Re" and the ground-state v=0 turning points shown by ().

1c. Calculated potential energy surfaces of BeAr.

2a. Calculated C $^1\Pi$ and c $^3\Sigma^+$ potential energy surfaces of MgAr, shifted to asymptotically match the experimental energies of ^1P and ^3P Mg, respectively.

2b. Calculated C $^1\Pi$ and c $^3\Sigma^+$ potential energy surfaces of CdAr, shifted to asymptotically match the experimental energies of ^1P and ^3P Cd, respectively.

2c. Calculated potential energy surfaces of BeAr, shifted to asymptotically match the experimental energies of ^1P, ^3P, and ^3S Be.

3. "Vibronic" coupling between a vibrational eigenstate of a bound $^1\Pi$ state and the isoenergetic continuum eigenstate of an underlying dissociative $^3\Sigma^+$ state.

4a. Morse potential vibrational eigenfunction for the v=0 vibrational level of C $^1\Pi$ MgAr and the isoenergetic continuum eigenfunction of the underlying c $^3\Sigma$ state.

4b. Morse potential vibrational eigenfunction for the v=7 vibrational level of C $^1\Pi$ MgAr and the isoenergetic continuum eigenfunction of the underlying c $^3\Sigma^+$ state.

5a. Morse potential vibrational eigenfunction for the v=0 vibrational level of C $^1\Pi$ CdAr and the isoenergetic continuum eigenfunction of the underlying c $^3\Sigma^+$ state.

5b. Morse potential vibrational eigenfunction for the v=11 vibrational level of C $^1\Pi$ CdAr and the isoenergetic continuum eigenfunction of the underlying c $^3\Sigma^+$ state.

Table I. Summary of Basis Sets and Effective Core Potentials.

	Ar	Ar[d]	Mg	Cd	Be
ECP[a]	SBK	None	None	HW	None
Basis[b]	SBK DZ	MC	MC	HW DZ	6-311G[c]
α_s	0.027	0.027	0.0209, 0.00825	0.02176	0.0285, 0.01125
α_p	0.021	0.021	0.0152, 0.0060	0.0162	0.0171, 0.00675
α_d	1.70, 0.425	1.70, 0.425	0.175	None	0.400

[a] "SBK" ("HW") denotes the ECP from reference 15 (18).

[b] "SBK DZ" ("HW DZ") denotes the double-zeta valence basis defined in reference 15 (18). "MC" denotes the McLean-Chandler (12s9p/6s5p) basis from reference 16.

[c] See reference 17.

[d] Used only in the BeAr all-electron calculations.

Table II. Calculated and Experimental Atomic Excitation Energies.[a]

Atom	$^1S \rightarrow {}^3P$	$^1S \rightarrow {}^1P$	$^1S \rightarrow {}^3S$
Mg	2.71	4.78	4.98
	(2.69)	(4.34)	(5.12)
Cd	3.38	5.51	5.85
	(3.73)	(5.42)	(6.37)
Be	3.08	6.20	6.37
	(2.73)	(5.29)	(6.46)

[a] In eV. Experimental values (taken from Moore, C.E. "Atomic Energy Levels", Vols. 1 and 3, Nat. Stand. Ref. Data. Ser., NBS, 1971) are given in parentheses.

Table III. Dominant Electron Configuration for Each Electronic State.

Electronic State	Configuration
$X\ ^1\Sigma^+$	$(ns)^2$
$A\ ^3\Pi$, $C\ ^1\Pi$	$(ns)^1(np_\pi)^1$
$c\ ^3\Sigma^1$, $D\ ^1\Sigma^1$	$(ns)^1(np_\sigma)^1$
$E\ ^3\Sigma^+$	$(ns)^1([n+1]s)^1$

Table IV. Values of Nuclear Wavefunction Overlap Integrals of MgAr.[a]

Vibrational Quantum Number	$\lvert\langle c\ ^3\Sigma^+ \mid C\ ^1\Pi \rangle\rvert$[b]	Percent of Maximum Overlap[b]
0	8.3×10^{-5}	0.10
1	2.6×10^{-4}	0.36
2	5.8×10^{-4}	0.87
3	1.1×10^{-3}	1.70
4	1.8×10^{-3}	2.92
5	2.6×10^{-3}	4.52
6	3.6×10^{-3}	6.52
7	4.6×10^{-3}	8.82

[a] All values are unitless.

[b] See text.

Table V. Values of Nuclear Wavefunction Overlap Integrals of CdAr.[a]

Vibrational Quantum Number	$\lvert\langle c\ ^3\Sigma^+ \mid C\ ^1\Pi\rangle\rvert$[b]	Percent of Maximum Overlap[b]
0	5.9×10^{-7}	0.00
1	4.2×10^{-7}	0.00
2	1.5×10^{-6}	0.00
3	2.3×10^{-6}	0.00
4	3.4×10^{-6}	0.01
5	6.7×10^{-6}	0.01
6	1.1×10^{-5}	0.02
7	1.8×10^{-5}	0.04
8	2.6×10^{-5}	0.06
9	3.6×10^{-5}	0.08
10	1.7×10^{-5}	0.11
11	5.9×10^{-5}	0.15

[a] All values are unitless.

[b] See text.

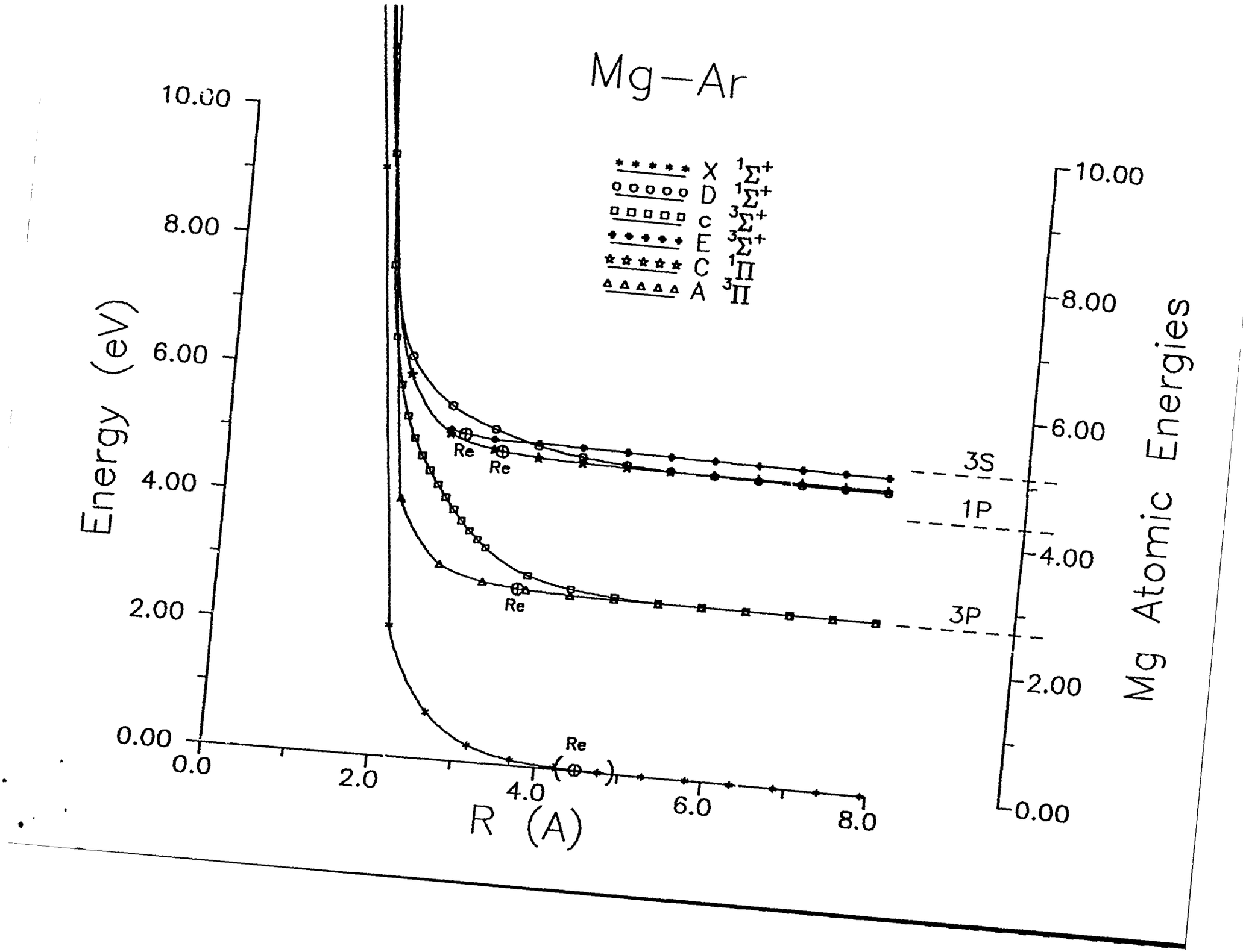
Mg–Ar
X $^1\Sigma^+$
D $^1\Sigma^+$
c $^3\Sigma^+$
E $^3\Sigma^+$
C $^1\Pi$
A $^3\Pi$
Re
Re
Re
Re
3S
1P
3P
Energy (eV)
10.00
8.00
6.00
4.00
2.00
0.00
0.0
2.0
4.0
6.0
8.0
R (A)
Mg Atomic Energies

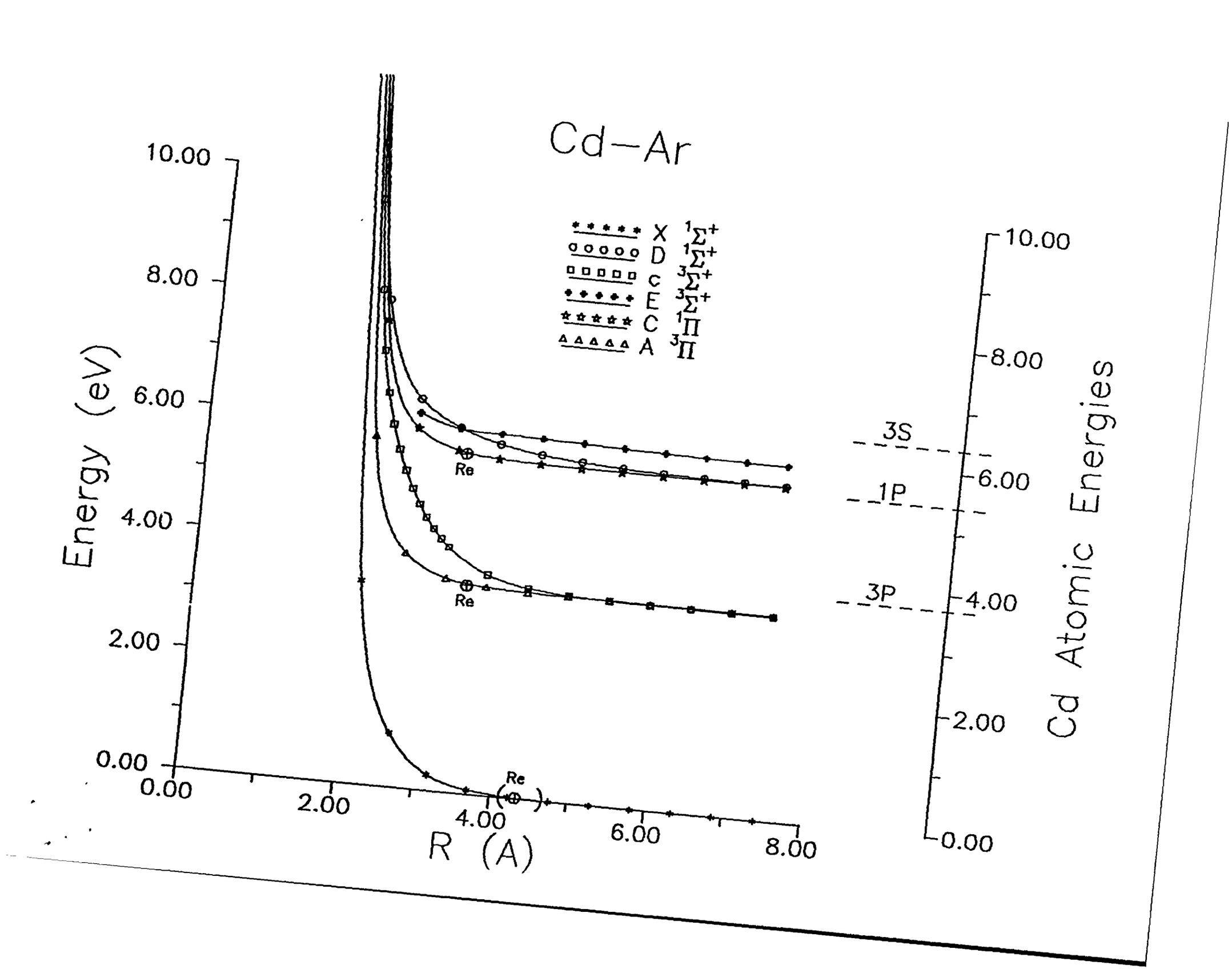
Cd–Ar
X $^1\Sigma^+$
D $^1\Sigma^+$
c $^3\Sigma^+$
E $^3\Sigma^+$
C $^1\Pi$
A $^3\Pi$
Re
Re
Re
Energy (eV)
10.00
8.00
6.00
4.00
2.00
0.00
0.00
2.00
4.00
6.00
8.00
R (A)
3S
1P
3P
Cd Atomic Energies

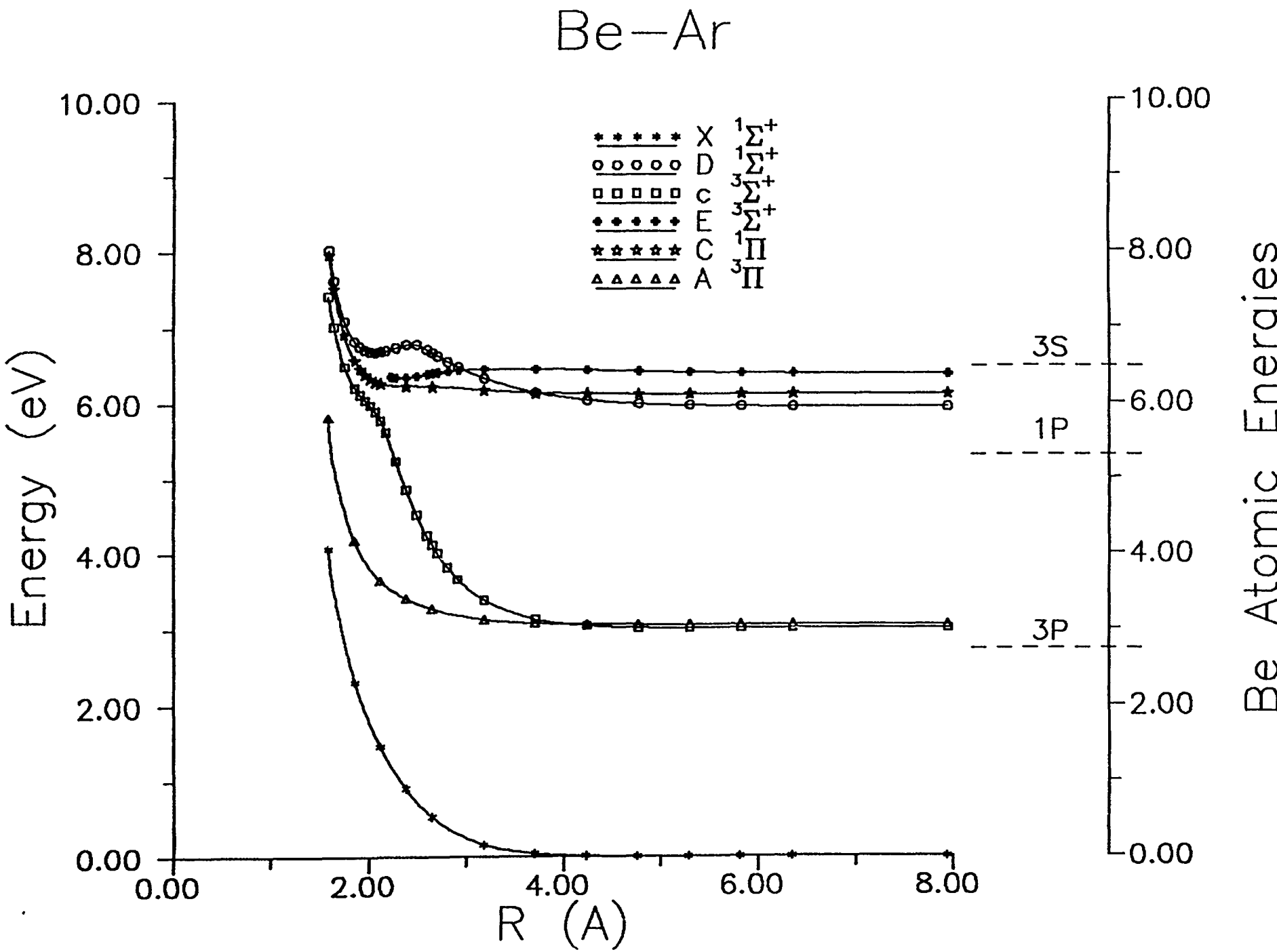
Be–Ar
X $^1\Sigma^+$
D $^1\Sigma^+$
c $^3\Sigma^+$
E $^3\Sigma^+$
C $^1\Pi$
A $^3\Pi$
3S
1P
3P
Energy (eV)
R (A)
Be Atomic Energies
10.00
8.00
6.00
4.00
2.00
0.00
0.00
2.00
4.00
6.00
8.00

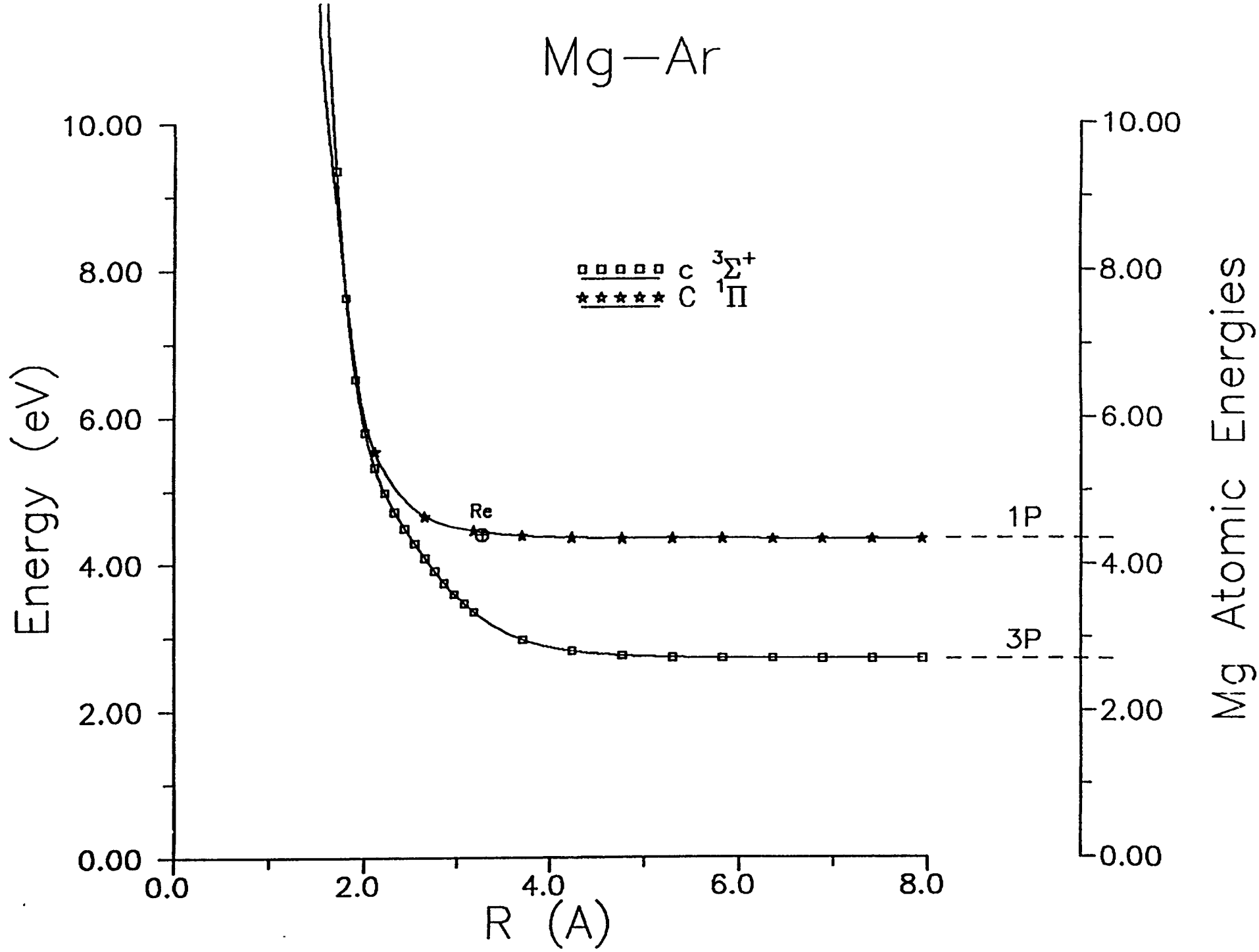
Mg—Ar
c $^3\Sigma^+$
C $^1\Pi$
Re
1P
3P
Energy (eV)
R (A)
Mg Atomic Energies
10.00
8.00
6.00
4.00
2.00
0.00
0.0
2.0
4.0
6.0
8.0

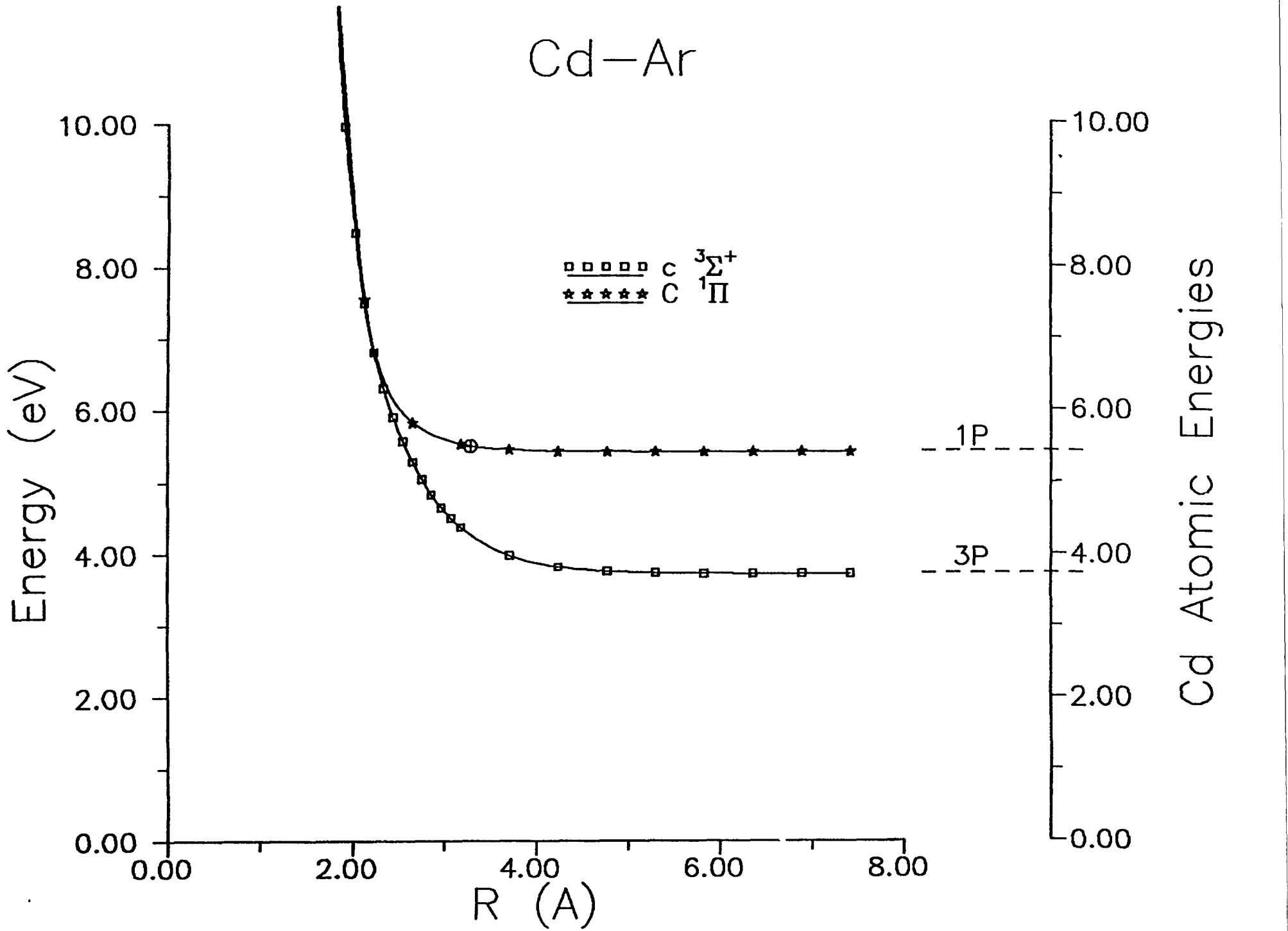
Cd—Ar
c $^3\Sigma^+$
C $^1\Pi$
1P
3P
Energy (eV)
R (A)
Cd Atomic Energies
10.00
8.00
6.00
4.00
2.00
0.00
0.00
2.00
4.00
6.00
8.00

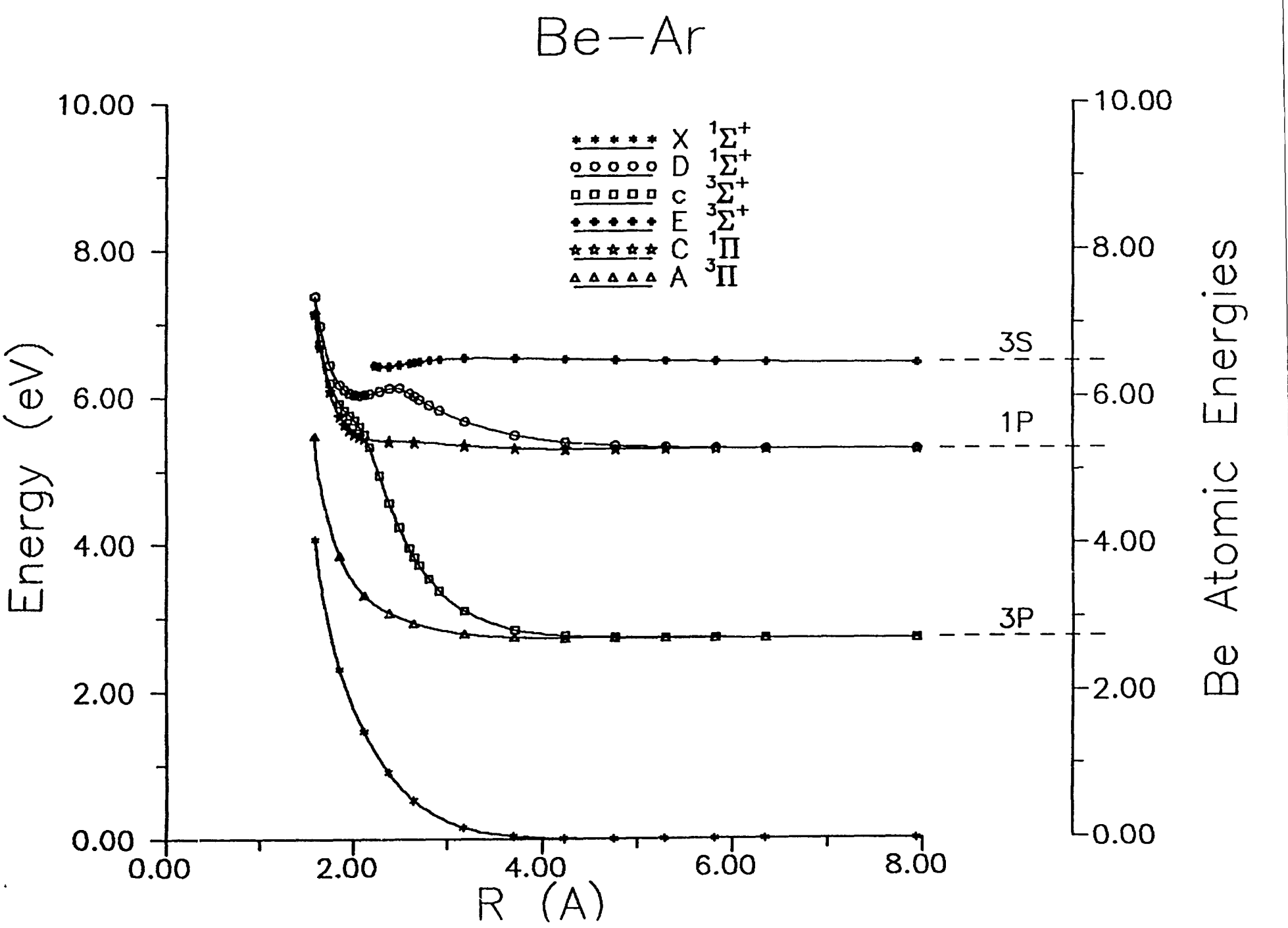
Be–Ar
X $^1\Sigma^+$
D $^1\Sigma^+$
c $^3\Sigma^+$
E $^3\Sigma^+$
C $^1\Pi$
A $^3\Pi$
3S
1P
3P
Energy (eV)
R (A)
Be Atomic Energies
10.00
8.00
6.00
4.00
2.00
0.00
0.00
2.00
4.00
6.00
8.00

E
R

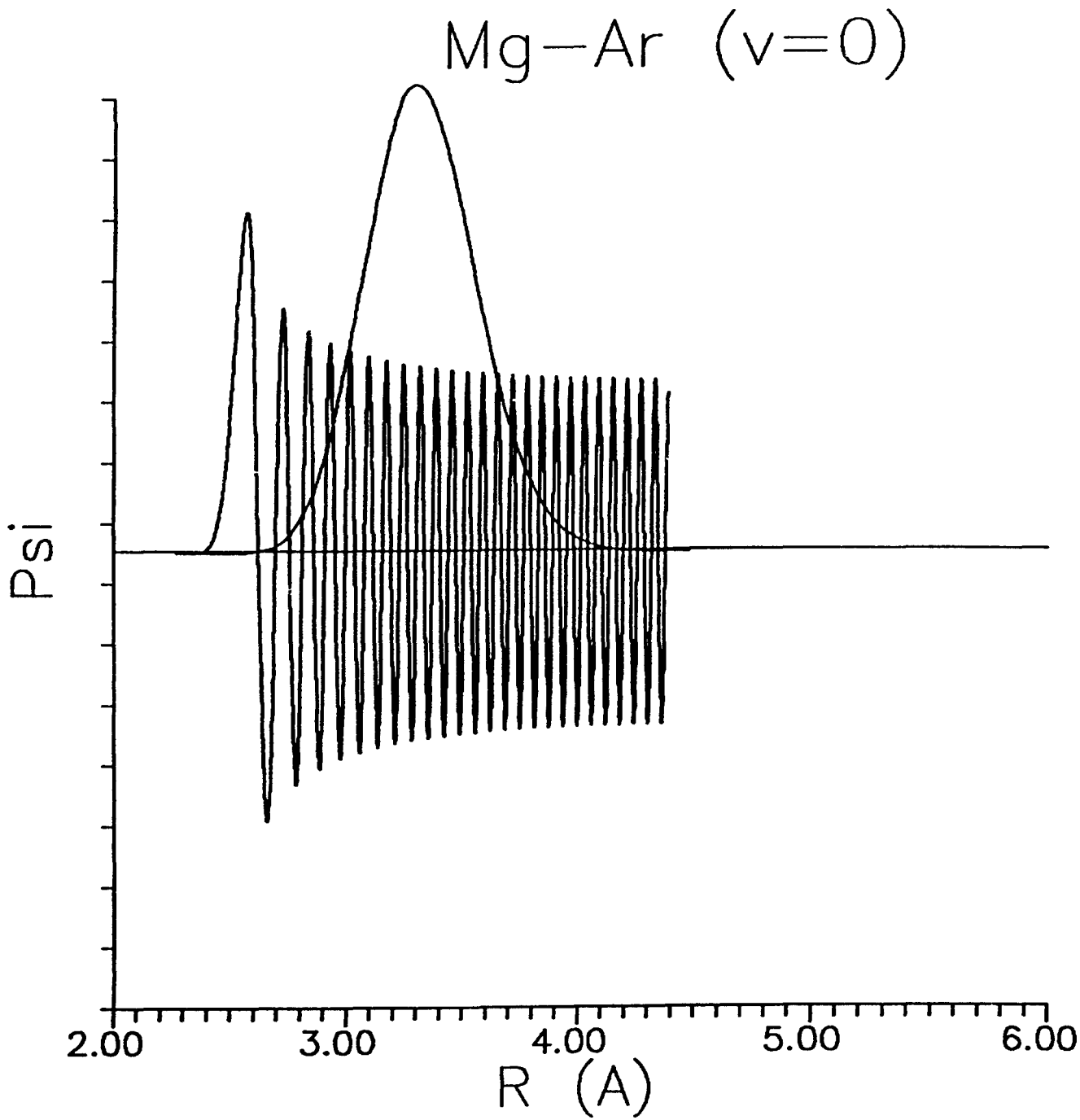
Mg–Ar (v=0)
Psi
2.00
3.00
4.00
5.00
6.00
R (A)

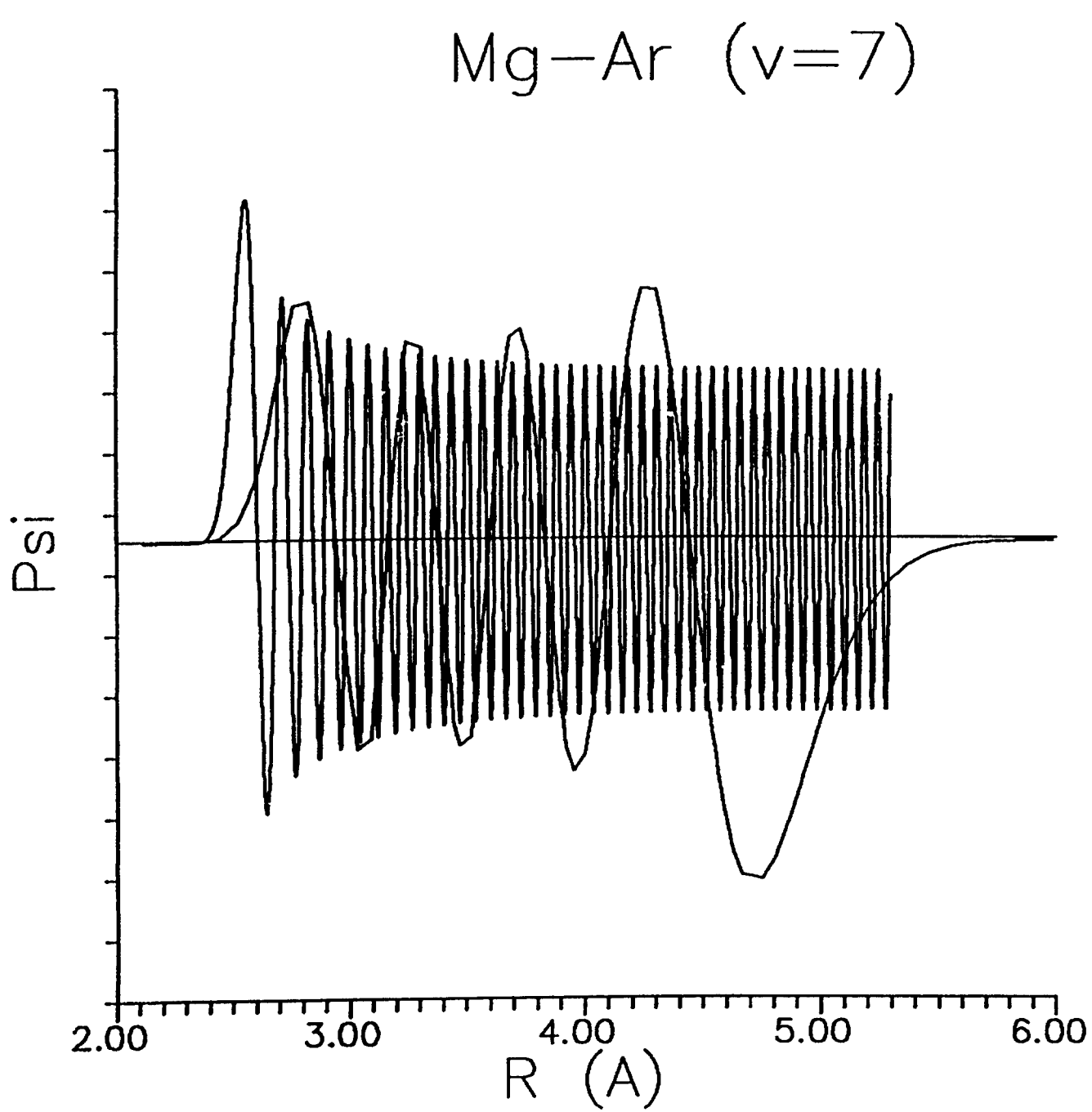
Mg–Ar (v=7)
Psi
2.00
3.00
4.00
5.00
6.00
R (A)

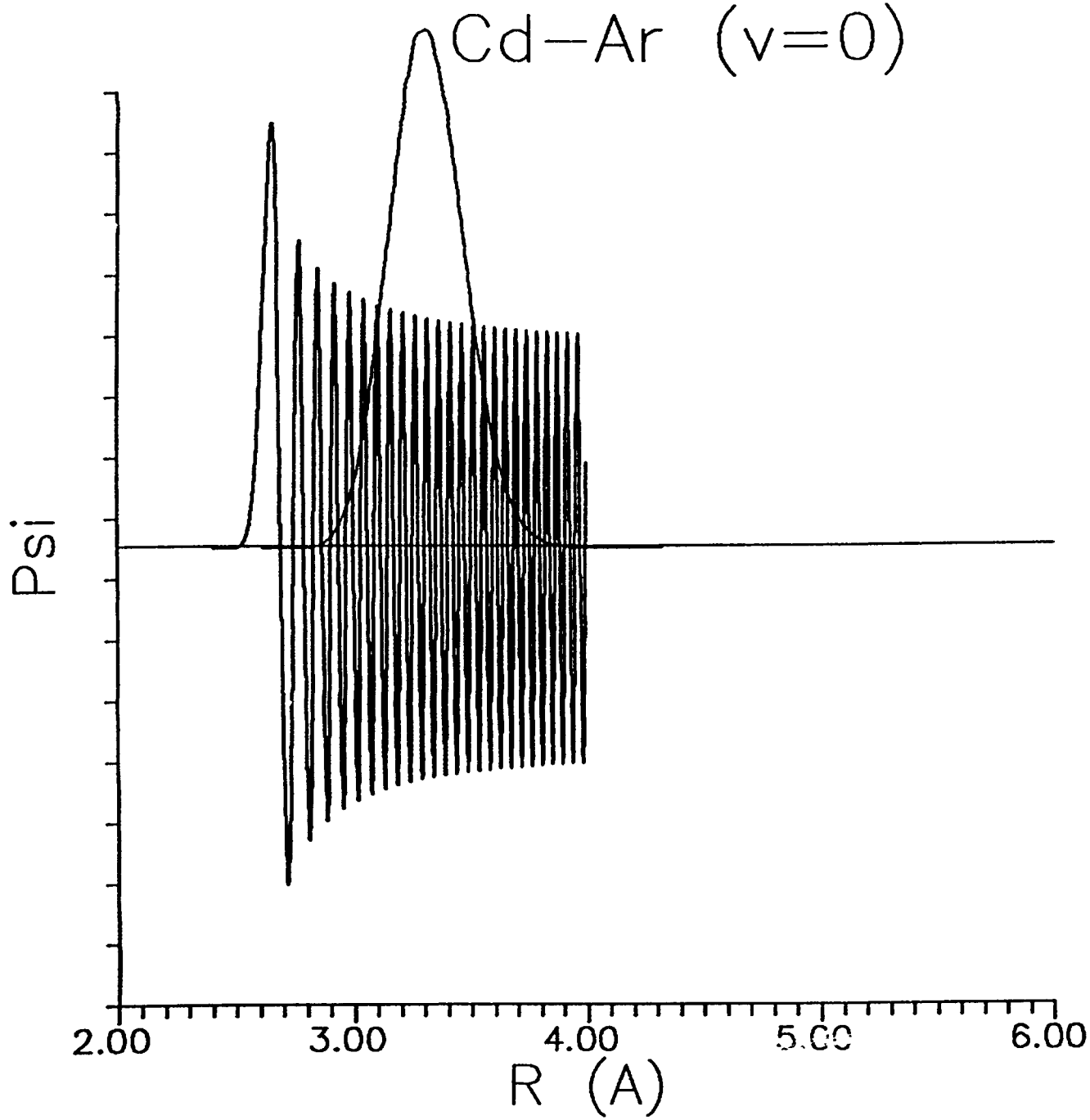
Cd–Ar (v=0)
Psi
2.00
3.00
4.00
5.00
6.00
R (A)

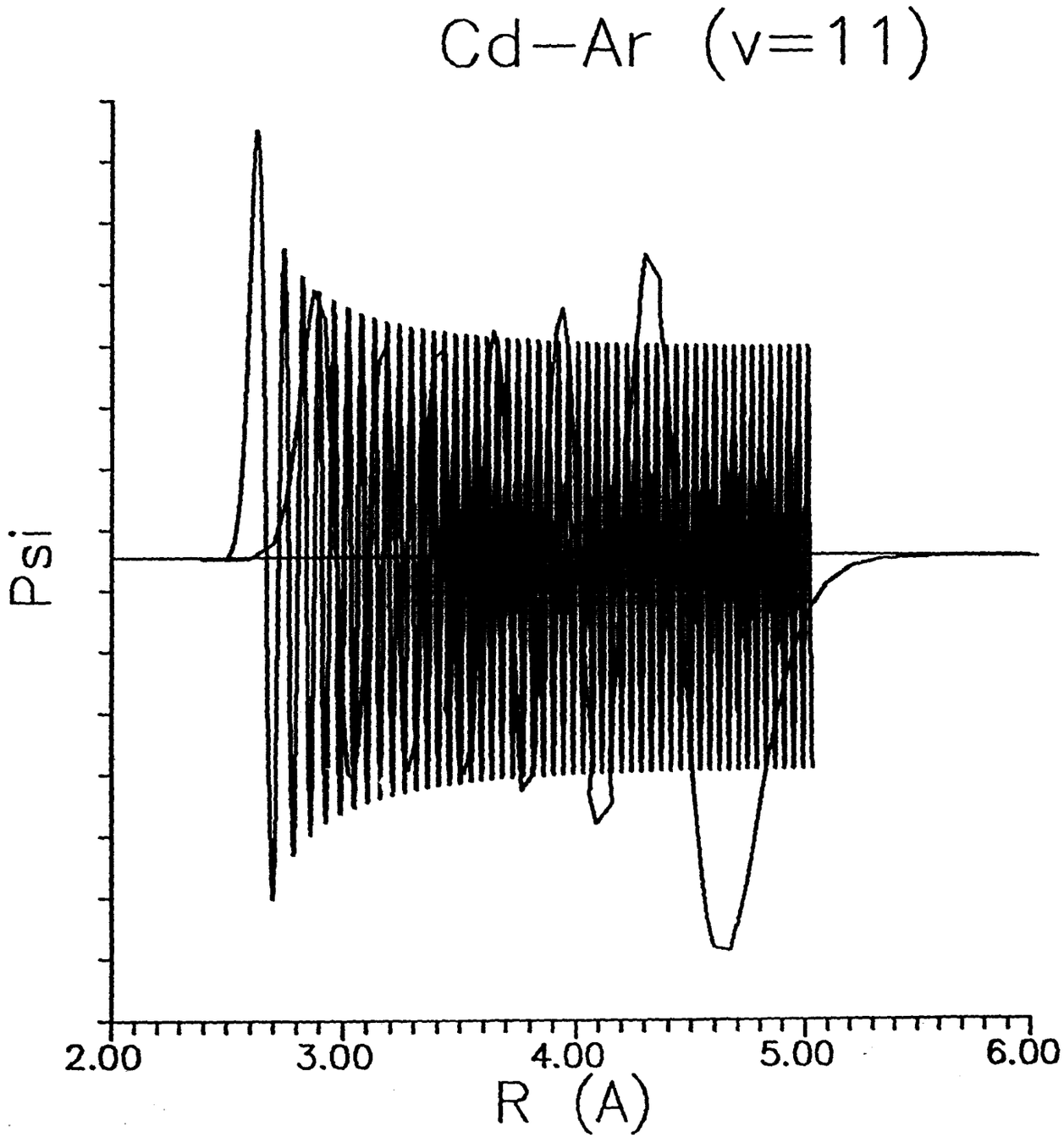
Cd–Ar (v=11)
Psi
2.00
3.00
4.00
5.00
6.00
R (A)